A Thermal–Hydraulic Comparison of Liquid Microchannel and Impinging Liquid Jet Array Heat Sinks for High-Power Electronics Cooling

Anthony J. Robinson

***Abstract*—In this paper, two single-phase liquid cooling strategies for electronics thermal management are compared and contrasted; impinging jet arrays and laminar flow in microchannels. The comparison is posed for a situation in which an electronic device must dissipate 250 W/cm^2 while being maintained at a temperature of 85 °C. The calculations indicate that both the impinging jet and microchannel heat sinks can provide the necessary cooling with less than 0.1 W of pumping power. Microchannels achieve this heat transfer target with such low pumping power by the relatively high pressure drop being offset by a low volumetric flow rate. In contrast, impinging jet heat sinks require a lower pressure drop and higher volumetric flow rate. From a practical point of view, lower operating pressure and larger mass flow rates are desirable characteristics, since they will be less prone to leakage and will provide better temperature uniformity across the heated component.**

***Index Terms*—Impinging jet cooling, liquid cooling, microchannel cooling.**

NOMENCLATURE

A	area (m^2).
A_r	surface area coverage in (4).
A_w	heater surface area (m^2).
C_o	constant in (7).
d	jet diameter (m).
D_H	hydraulic diameter (m).
f	friction factor.
g	gravitational acceleration (m/s^2).
H	distance between orifice plate and impingement surface/height of channel (m).
h	surface averaged heat transfer coefficient (W/m^{2}K).
K	minor loss coefficients.
k	thermal conductivity (W/mK).
$L*$	characteristic length in (1) (m).
L_e	length of a unit cell in (1) (m).
L	heater length (m).
$\dot{m}$	mass flow rate (kg/s).
N	number of jets/channels (-).
Nu	Nusselt number (-).
ΔP	Pressure drop across orifice (Pa).
Pr	Prandtl number (-).
Q_{pumping}	pumping power (W).
q''_w	wall heat flux, (W/m^2).
R	thermal resistance (°C/W).
Re	Reynolds number (-).
S	jet-to-jet spacing (m).
t	thickness of nozzle plate or thickness of channel wall (m).
T	temperature (°C or K).
V	velocity (m/s).
$\dot{V}$	volumetric flow rate (m^3/s).
w	width of channel (m).

Subscripts:

c	cold (inlet).
f	fluid.
H	hot (outlet).
IJ	impinging jet.
j	jet.
MC	microchannel.
w	wall.

Greek:

μ	dynamic viscosity (kgm/s).
ρ	density (kg/m^3).
ν	kinematic viscosity (m^2/s).

Manuscript received December 19, 2007; revised November 24, 2008. First published March 16, 2009; current version published July 22, 2009. This work was supported by the Center for Telecommunications Value-Chain Research (CTVR), a CSET of Science Foundation Ireland. This work was recommended for publication by Associate Editor B. Sammakia upon evaluation of the reviewers comments.

A. J. Robinson is with the Department of Mechanical and Manufacturing Engineering and the CTVR, Lloyd Institute, Trinity College Dublin, Dublin 2, Ireland (e-mail: arobins@tcd.ie).

Digital Object Identifier 10.1109/TCAPT.2008.2010408

I. INTRODUCTION

IT is well known that thermal issues are presenting a severe bottleneck with regard to the advancement of electronic devices and components. With the predictions of Moore's Law generally being a reality, the density of transistors being packed onto chips is becoming so large that the thermal power densities are escalating to levels exceeding 100 W/cm^2. In the very near future, heat fluxes approaching 300 W/cm^2 will need to be dissipated [1]. These power densities far exceed the capabilities

of conventional low-tech fan-finned heat sinks [2]. This is due to several constraining issues which includes, but is not limited to, fin efficiency, fan acoustic emissions, fan power consumption, and electronic packaging/miniaturization issues. What will likely be required for the next generation of high-powered electronic devices are low-profile and low power consumption liquid cooling thermal hardware [3].

There are several liquid cooling techniques that are viable cooling strategies for electronics thermal management. These include passive two-phase systems such as immersed boiling/thermosyphons and heat pipes, as well as forced two-phase strategies such as two-phase forced convection in microchannels, looped heat pipes and capillary pumped loops. Heat pipes are a well established and mature technology with regard to electronics thermal management and have proven to be efficient and reliable. However, the tubular heat pipes must be embedded in a metallic block that is pressed onto the electronic component with a layer of thermal interface material (TIM) between the electronic device and the next level of thermal hardware. Since the thermal resistance of the TIM material can take up to 50% of the available thermal budget [4], even the heat pipe solution will soon become unusable as the heat flux levels continue to escalate. The other two-phase strategies offer the desirable properties of very high heat transfer coefficients, temperature homogenization, and passive or low power consumption during operation. Furthermore, they can be deployed as direct contact and "water-block" type solutions. In the latter, the thermal hardware is a separate and detachable sealed unit and will require a TIM to fix it to the electronic component. With the exceptionally low thermal resistance of two-phase heat transfer devices, the relative contribution of the TIM solution to the overall thermal resistance will become much larger. There is a great deal of effort being put forth to develop new TIM technologies to mitigate this fact [5]. In direct contact application there is no need for a TIM which significantly reduces the overall thermal resistance of the thermal hardware solution. However, the current capability to predict the heat transfer and critical heat flux levels during pool and convective boiling are unreliable. This, coupled with the fact that the thermal package must be compact and low profile at board level, leads to significant uncertainty regarding the reliability of two-phase thermal management solutions and hence the reluctance of electronic packagers to employ this type of technology.

In the near term, it is more likely that single-phase liquid cooling strategies will be implemented to dissipate the required heat flux levels generated by electronic components. In fact, there already exists a large number of commercially available devices that utilize a liquid reservoir, pump, water-block and air-cooled heat sink as the thermal management solution for high-powered devices. These devices force a high volume of relatively low velocity water over extended internal surfaces within the water-block. The extended internal surface area serves to adequately decrease the overall thermal resistance of the device. However, the extended surface area combined with increased mixing of the flow tends to dramatically increase the required pumping power of the device. Furthermore, the extended internal surface area approach is not feasible for direct contact liquid cooling which may be required as heat flux levels exceed the 200 W/cm^2 mark.

Two single-phase forced liquid cooling strategies that show considerable promise for the cooling of high heat flux electronic devices are microchannel and impinging jet heat sinks. Liquid jet impingement is attractive for high power density applications because it provides the highest known single-phase heat transfer coefficient and is only really outstripped by convective boiling. Furthermore, when arranged in arrays, this technique offers very good temperature uniformity over the jet impingement surface [6]. One of the major shortcomings of liquid jet array impingement heat transfer is the fact that it has not been adequately characterized in the open literature [6]. Although there is a significant body of work for single air and liquid jets, the works of Jiji and Dagan [7], Pan and Webb [8], Womac *et al.* [9], Fabbri and Dhir [10], and Robinson and Schnitzler [11] are the works that provide practical design correlations for the prediction of the average heat transfer coefficient for liquid jet arrays. Further to this, only the works of Womac *et al.* [9] and Robinson and Schnitzler [11] provide correlations for confined and submerged jet array impingement heat transfer, with the others considering free surface jets. The latter also provided information about the pressure drop characteristics. Considering that a compact and low-profile thermal package will most likely require that the jets be confined and submerged, combined with the fact that confined jets with a small jet to target spacing have a considerably larger heat transfer coefficient compared with free jets, only confined submerged jets will be discussed in this paper. Reviews of free-surface liquid jet arrays can be found in [10], [11].

Womac *et al.* [9] were perhaps the first to adequately quantify and correlate confined-submerged jet array impingement heat transfer. In this paper, both water and FC-77 were used as the coolants. Arrays of 2×2 and 3×3 circular jets were tested for jet diameters of $d = 0.513$ mm and $d = 1.02$ mm over various jet-to-jet spacing. Experiments conducted for the confined-submerged liquid jet arrays found that the heat transfer coefficient was somewhat insensitive to jet-to-target spacing, H, within the range of $2 \leq H/d \leq 4$. Heat transfer to the impinging jets was generally found to diminish for small $(H/d \leq 2)$ and large $(H/d \geq 10)$ separations, depending on jet-to-jet spacing. The submerged jets were found to perform equally, if not better, than their free jet counterparts under similar flow conditions. An area weighted combination of expressions for the impingement and wall jet regions over the entire heated surface was correlated as

$$\frac{\mathrm{Nu}_L}{\mathrm{Pr}^{0.4}} = 0.509\,\mathrm{Re}_d^{0.5}\left(\frac{L}{d}\right)A_r + 0.0363\,\mathrm{Re}_{L^*}^{0.8}\left(\frac{L}{L^*}\right)(1-A_r) \tag{1}$$

where L is the heater length, $L^* = 0.25(\sqrt{2}+1)L_e - (1.9d)$ is an estimate of the average distance affiliated with radial flow in the wall jet regions, and $A_r = N\pi(1.9d)^2/L^2$ is the ratio of the effective area of the impingement regions on the heater to the total area of the surface.

Robinson and Schnitzler [11] investigated water jet impingement cooling for both free-surface and confined-submerged jet arrays. Jet diameters of 1.0 mm were used with varying jet-to-jet spacing of $S = 3, 5$, and 7 jet diameters. Averaged heat transfer and pressure drop data were recorded for dimensionless jet-to-target spacings of $2 \leq H/d \leq 30$ and volumetric flow rates in the range of $2\,L/\mathrm{min} \leq \dot{V} \leq 9\,L/\mathrm{min}$.

For the confined and submerged jets, it was reported that heat transfer was insensitive to jet-to-target spacing in the range of $2 \leq H/d \leq 3$. A monotonic decrease in heat transfer was observed with increasing jet-to-target spacing in the range of $5 \leq H/d \leq 20$. It was reported that for a constant Reynolds number, increasing the jet-to-jet spacing incurred a detrimental effect on heat transfer. It was also noted that a stronger dependence on jet-to-jet spacing was encountered for smaller jet-to-target spacing. For small jet-to-target spacing $(2 \leq H/d \leq 3)$, Robinson and Schnitzler [11] correlated their average heat transfer data for confined-submerged jets as

$$\mathrm{Nu}_d = 1.485\,\mathrm{Re}_d^{0.46}\left(\frac{S}{d}\right)^{-0.442}\left(\frac{H}{d}\right)^{-0.00716}\mathrm{Pr}^{0.4}. \quad (2)$$

The correlation was found to agree very well with the correlation of Womac *et al.* [9] given by (1). Further to this the friction factor was correlated as

$$f = 0.51 + \frac{229.9}{\mathrm{Re}_d}. \quad (3)$$

Equation (3) was found to be in close agreement with that of Fabbri and Dhir [10] albeit the latter work was performed for the impingement of free surface microjets. With regard to the continual operating cost of the thermal management hardware, the relationship between the heat transfer coefficient and the required pumping power was investigated. For the confined-submerged jet arrays, Robinson and Schnitzler [11] found that increasing the number of jets had the effect of decreasing the required pumping power to achieve a target heat transfer coefficient.

One of the promising areas of research with regard to jet impingement heat transfer results from the fact that the nozzle plate within which the jet orifices pass are typically thin enough that the pressure drop across the nozzle is primarily due to the entrance and discharge losses. Consequently, variations in the orifice entrance or exit can have rather profound effects on the pressure drop and may not significantly alter the heat transfer. Work by [12]–[16] have all shown that significant improvement in the required pressure drop can be realized with simple changes to the inlet and outlet geometries of the jet orifice with small influence on the heat transfer coefficient.

Compared with jet impingement heat transfer, microchannel heat sinks have been studied in much greater detail. This is likely due to the fact that it is possible to manufacture the microchannel heat sink directly onto the silicon die, effectively integrating the cooling solution at die level with the electronic circuitry of the device. In general, single-phase flow in microchannels has a lower surface averaged heat transfer coefficient compared with impinging jets. However, the shortfall in the heat transfer coefficient can be compensated by the fact that the coolant is exchanging energy with a larger effective surface area due to the multiple walls within each of the microchannels. Although microchannel heat transfer and pressure drop has received far greater attention compared with the impinging jet counterpart, the trouble is that there currently exists a huge discrepancy between the measurements of different investigations for both the heat transfer and friction factor. Detailed reviews of microchannel flow and heat transfer can be found in [17] and [18]. Of particular interest for this investigation is the comprehensive review of single-phase flow and heat transfer provided by Morini [17]. In this review paper, 29 single-phase microchannel heat transfer investigations were detailed. For rectangular channels it was determined that the majority of the investigations, some 75%, measured average heat transfer coefficients that were in agreement with, or notably less than, what would be predicted by established macrochannel correlations. With regard to pressure drop, a similar outcome was revealed. Morini [17] showed that for laminar flow the majority (87%) of the available microchannel investigations measured Poisselle numbers (fRe) that agreed with or were in excess of that predicted for macrochannel flows. Physical explanations for the observed discrepancies in the literature are under debate although they are likely due to factors such as entrance effects, axial conduction, conjugate heat transfer, measurement uncertainty, surface roughness, and variable thermophysical properties [18]. This has been established by a few works [18]–[20] in which numerical simulations of microchannel flow and heat transfer are debunking the existence of "special micro-effects" and showing that the Navier–Stokes equations accurately predict microscale flow and heat transfer. Herwig and Hausner [18] showed that large gradients in the bulk liquid and wall temperatures explained the surprising Nusselt number results that Tso and Mahulikar [21] determined experimentally which were believed to be caused by a so-called micro-effect. Li *et al.* [19] and Li *et al.* [20] have shown that variable thermophysical properties can strongly influence both the flow and heat transfer in microchannel heat sinks. In Li *et al.* [20] the changes in the physical properties with temperature were accounted for in the numerical simulations for a thermally and hydrodynamically developing flow and very good agreement was observed with well established macrochannel correlations that accounted for this change along the length of the channel and poor agreement was generally observed with those correlations that did not. The use of the Sieder and Tate [22] and Hausen [23] correlations are often suggested to account for entrance and property variations [24], [25]. In Li *et al.* [20], the surface average heat transfer coefficients from the numerical simulations showed particularly good agreement with the correlation developed by Sieder and Tate [22] for laminar flow with a combined entry length. The Sieder and Tate correlation is expressed as

$$\mathrm{Nu}_{D_H} = 1.86\left(\frac{\mathrm{Re}\,\mathrm{Pr}\,D_H}{L}\right)^{0.33}\left(\frac{\mu_f}{\mu_w}\right)^{0.14} \quad (4)$$

where D_H is the hydraulic diameter and L is the length of the channel. Equation (4) is approximately valid for situations in which $(\mathrm{RePrD}_H/L)^{1/3}(\mu_f/\mu_w)^{0.14} > 2$ [25] and the term $(\mu_f/\mu_w)^{0.14}$ had been added to partially account for changes in the liquid viscosity due to heating of the liquid along the channel. Furthermore, all properties are evaluated at the average liquid temperature between the inlet and outlet, except μ_w which is evaluated at the wall temperature.

In this investigation, the heat transfer and pressure drop of single-phase impinging liquid jet arrays and microchannel heat sinks are considered. Given the state of the available information in the open literature, with impinging liquid jet arrays being under-characterized and liquid microchannels being over-characterized to the point of contradiction, it seems instructive to

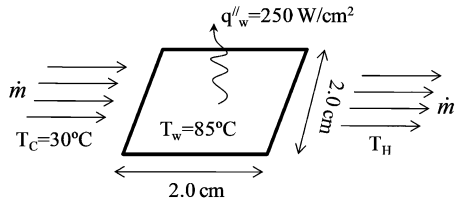

Fig. 1. Test surface to be used in the comparison of the two liquid-cooled heat sinks.

compare and contrast the two potential technologies in the least conservative scenario. Due to the limited information available, the correlations of Robinson and Schnitzler [11] will be utilized to characterize the submerged and confined impinging liquid jet arrays. To provide the least conservative comparison, the microchannel heat transfer and friction factor will be predicted using correlations developed for macrochannel flow since they should render the highest heat transfer coefficient for the lowest pressure drop.

II. Analysis

A. Test Case

Considering the extremely wide range of electronic components found in application, it is not feasible to make comparisons that cover all of the possible geometric and thermal scenarios that may be encountered in reality. For comparison of the two single-phase liquid cooling techniques considered here, one rather extreme and practical test case will be considered. As depicted in Fig. 1, a square shaped electronic component of dimensions 2.0 cm × 2.0 cm will be considered. The heat flux level to be dissipated will be $q'' = 250$ W/cm^2, which can be considered quite high considering the state-of-the-art. A further thermal constraint is that the wall temperature must be kept below a maximum of $T_w = 85$ °C. Further to this, it will be assumed that the inlet liquid temperature to the respective heat sink will be constant at $T_c = 30$ °C, presumably returned from a remote air-cooled heat sink similar to that developed by Bintoro *et al.* [26] or Harris *et al.* [27].

B. Impinging Liquid Jet Arrays

As previously stated, the heat transfer and friction factor correlations provided by Robinson and Schnitzler [11] will be used in this comparative study. The correlations (2) and (3) were developed for a Reynolds number range of $600 \leq \mathrm{Re}_d \leq 6000$ although recent experimental work has extended this Reynolds numbers to over 10 000 [13]–[15]. Dimensionless jet-to-jet spacing between $3 \leq S/d \leq 7$ and dimensionless jet-to-target spacing of $2 \leq H/d \leq 3$ were tested. The correlations were developed for a fixed jet diameter of $d = 1.0$ mm. However, excellent agreement with the Womac *et al.* [1] correlation, which is applicable for diameters down to 0.5 mm, suggests that the Robinson–Schnitzler heat transfer correlation can be applied to microscale diameters with reasonable accuracy. Likewise, the friction factor correlation was virtually identical to that developed by Fabbri and Dhir [10] for microscale free surface jets, lending credibility to the use of (3) outside of the diameter range for which it was developed. To simplify the analysis, the very weak dependence on the jet-to-target spacing will be ignored for $2 \leq H/d \leq 3$ such that (2) simplifies to

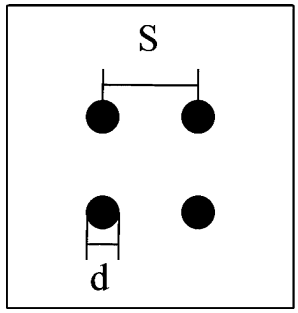

Fig. 2. Layout of the jet orifices within the nozzle plate.

$$\mathrm{Nu}_d = 1.485\,\mathrm{Re}_d^{0.46}\left(\frac{S}{d}\right)^{-0.442}\mathrm{Pr}^{0.4}. \tag{5}$$

The geometric parameters that affect the heat transfer and pressure drop characteristics of impinging liquid jet arrays are the jet diameter d, the jet-to-jet spacing S, and the number of jets that populate the nozzle N. These are depicted in Fig. 2 for a segment of the nozzle plate.

For simplicity, an uncomplicated relationship between the number of jets N and the jet-to-jet spacing S on the square 2.0 cm × 2.0 cm surface is

$$S(\sqrt{N} - 1) = 1.9. \tag{6}$$

Here, the effective length of 1.9 cm on the right-hand side of (9) has been obtained by not allowing jet centers to be placed beyond a 0.5-mm-thick border around the inside of the outer edge of the surface. In this way, the jets ($0.3\ \mathrm{mm} \leq d \leq 1.0\ \mathrm{mm}$) cannot overlap the edge of the target surface.

Combining (5) and (6) and rearranging gives a simplified expression of the heat transfer coefficient in terms of the total volumetric flow rate, jet diameter, and total number of jets

$$h = C_o \dot{V}^{0.46} d^{-1.018}\left[\frac{(\sqrt{N}-1)^{0.442}}{N^{0.46}}\right] \tag{7}$$

where the term C_o is a grouping of constants and physical properties which, for the test case of this study, is calculated as

$$C_o = 8.56 k_f \left(\frac{4}{\pi \upsilon}\right)^{0.46}\mathrm{Pr}^{0.4} = 7879. \tag{8}$$

Equation (7) indicates that for fixed jet diameter and jet population, the heat transfer coefficient increases asymptotically with the total volumetric flow rate of water passing across the nozzle plate. This is depicted in Fig. 3 for a fixed $N = 100$ jets and jet diameters ranging between $0.3\ \mathrm{mm} \leq d \leq 1.0$ mm. It is also evident that the heat transfer coefficient is inversely proportional to the jet diameter. This is partially due to the fact that decreasing the diameter for a fixed volumetric flow rate and jet population increases the velocity and thus the heat transfer to

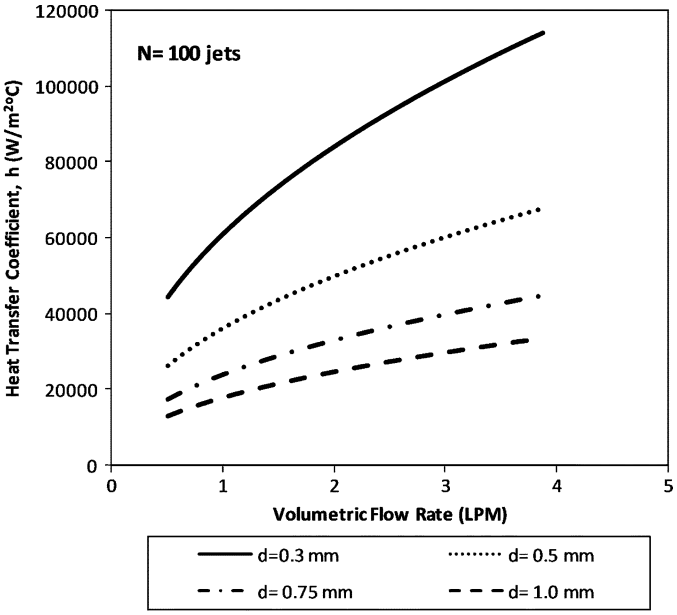

Fig. 3. Variation of the heat transfer coefficient with the total volumetric flow rate and jet diameter for $N = 100$ jets.

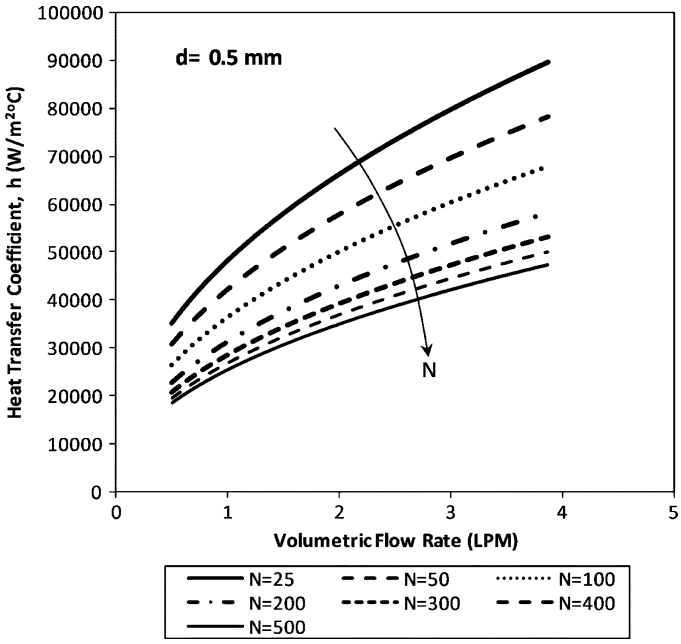

Fig. 4. Variation of the heat transfer coefficient with the total volumetric flow rate and jet populations for a $d = 0.5$-mm-diameter jet orifice.

each respective jet. Fig. 3 illustrates that the sensitivity to jet diameter can be quite extreme for the smaller diameters and tends to diminish as the jets become larger.

The final bracketed term in (7) indicates that the heat transfer coefficient depends on the number of jets that impinge on the surface with an approximate dependence of $h \sim 1/N^{0.25}$. Thus, for a fixed volumetric flow rate and jet diameter, decreasing the population of jets increases the heat transfer coefficient. This is due to the increase in the issuing jet velocity of the jets that compensates for the loss of overall surface coverage. This is illustrated in Fig. 4 for a fixed jet diameter of $d = 0.5$ mm. Again, the sensitivity to changes in the jet population N tends to decrease as N increases. It must be cautioned that this trend is only likely for relatively close jets $H/d < 10$. Although this has yet to be quantified for confined and submerged jets, the rate at which the Nusselt number decreases with increasing S/d will most probably become much larger once the jets are far enough away from each other that neighboring jets no longer interact significantly, as has been confirmed for measurements of free surface jet arrays [10].

For the test case considered here, the required heat transfer coefficient to achieve the thermal constraints of $q''_w = 250$ W/cm^2 and $T_w = 85°$C can be determined as

$$h = \frac{\mathrm{Nu}_d k_f}{d} = \frac{q''_w}{(T_w - T_j)} = 45\,454 \quad \frac{W}{m^{2\circ}C}. \tag{9}$$

This is achieved by forcing water jets to impinge on the heated surface with jet velocities of

$$V = \frac{4\dot{V}}{N\pi d^2}. \tag{10}$$

The corresponding jet Reynolds number is

$$\mathrm{Re}_d = \frac{Vd}{\upsilon_f}. \tag{11}$$

The pressure drop required to form the jets is calculated from the expression

$$\Delta P = f\left(\frac{1}{2}\rho V^2\right)\left(\frac{t}{d}\right) \tag{12}$$

where t is the thickness of the nozzle plate, and the friction factor f is calculated using (3). The required pumping power is thus

$$Q_{\mathrm{pumping}} = \dot{V}\Delta P. \tag{13}$$

In all of the above expressions, the fluid properties have been evaluated at the water film temperature of $T_f = 330$ K.

By combining the above set of equations with (2) and (3), it is possible to derive an expression that predicts the pumping power that is necessary to provide the heat transfer coefficient that will dissipate the heat flux of 250 W/cm^2 (i.e., $h = 45\,454$ W/m$^{2\circ}$C) in terms of only the jet diameter and the total number of jets. For the test case considered here this expression is

$$Q_{\mathrm{pumping}} = \frac{Nd^{0.426}}{(\sqrt{N}-1)^{1.92}}\left[112269\,\frac{d^{1.213}}{(\sqrt{N}-1)^{0.96}} + 0.422\right]. \tag{14}$$

Equation (14) is plotted in Fig. 5 for varying jet diameter d and jet population N. It is clear that increasing the jet diameter increases the required pumping power for a given jet population. The slope of the Q_{pumping} versus d curves is steeper for smaller jet populations. It is also evident that, for a fixed jet diameter, increasing the jet population from $N = 25$ to $N = 300$ has a profound effect on the pumping power. However, in the region between $300 \leq N \leq 500$, the effect of increasing N is not as severe. In general, the analysis tends to indicate that in order to achieve the target heat transfer rate with the smallest pumping power, tightly packed jets with as small as practical diameter are required. For example, $N = 500$ microjets with diameters in the

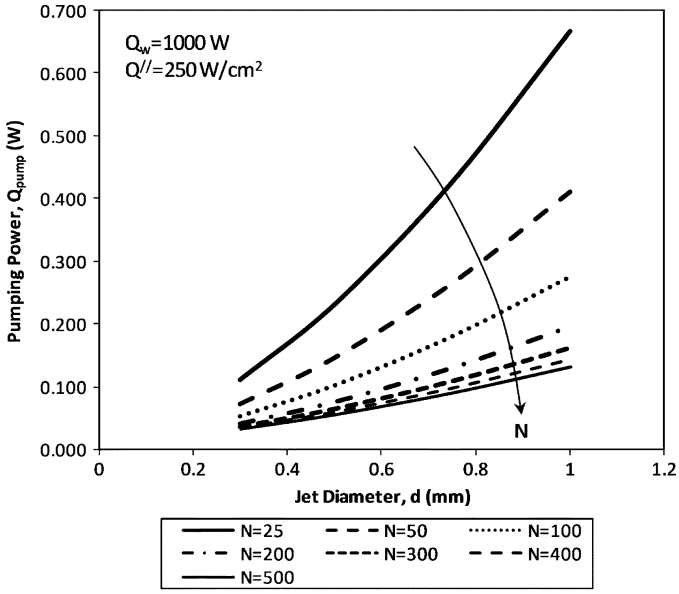

Fig. 5. Variation of the pumping power requirement to achieve a heat flux removal rate of 250 W/cm^2 with varying jet diameter and jet population.

range of $d = 300\ \mu$m to $d = 500\ \mu$m will only require pumping power in the range of $0.033\ \text{W} \leq Q_{\text{pumping}} \leq 0.056\ \text{W}$ which is minimal considering that the electronic component in this case is dissipating 1000 W.

C. Microchannel Heat Sinks

As stated earlier, the heat transfer and friction factor correlations that have been developed for laminar flow in macrochannels will be used in this comparative study. The motivation for this is to provide a large thermal–hydraulic division between the two liquid cooling techniques to determine if one technology far outstrips the other. To achieve this, the heat transfer correlation provided by Sieder and Tate [22] for thermally and hydrodynamically developing laminar flow (4) will be used. The primary reason for this decision is that its predictive capability has been validated by recent numerical simulations as discussed earlier. Morini [17] indicates that the conventional theory for the friction factor for fully developed flow through rectangular microchannels can be calculated as

$$f = \frac{C(\gamma)}{\text{Re}_{D_H}} \tag{15}$$

where the coefficient ranges between $56.92 \leq C(\gamma) \leq 96$ depending on the rectangular aspect ratio, $\gamma = w/H$ or H/w, whichever is smaller [6]. The pressure drop along the channel is predicted by

$$\Delta P = f\left(\frac{1}{2}\rho V^2\right)\left(\frac{L}{D_H}\right) + K\left(\frac{1}{2}\rho V^2\right). \tag{16}$$

The constant K is the minor loss coefficient which has been estimated as $K = 1.5$, with a minor loss coefficient of 0.5 for the entrance into the square channel and 1.0 for a sudden expansion at the exit [27].

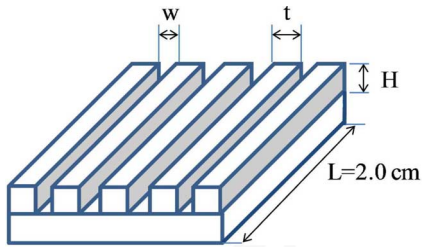

Fig. 6. Geometric layout of a microchannel array.

For the test case considered here, the geometric parameters that influence the heat transfer and pressure drop characteristics within the liquid microchannel heat sinks are the channel width w, channel height H, and the number of channels that are packed onto the heater surface N, as depicted in Fig. 6.

The maximum number of microchannels of width w that can exist on a square surface of length $L = 2.0$ cm can be determined provided that the thickness of the wall that separates the channels t is given. Here, the thickness of the separating wall between channels is to be assumed constant at $t = 50\ \mu$m, which can be considered quite thin. In a similar manner to that of the microjets, the number of channels N can be related to the channel width w with the expression

$$wN + (N+1)t = 2.0\,\text{cm}. \tag{16}$$

This expression ensures that walls, and not channels, are placed at the ends of the heat sink. Furthermore, it will be assumed that the flowing liquid exchanges thermal energy with the bottom surface of the channel as well as the two side walls. The top wall is assumed to be adiabatic since it is typically a covering plate [6]. Consequently, for a single channel the total exposed area for heat transfer is

$$A = wL + 2HL. \tag{17}$$

A further simplification is that all three walls are nearly isothermal and at $T_w = 85\ ^\circ$C. This is equivalent to assuming a fin efficiency of 100% which should provide the least conservative estimate of the heat transfer although the general trends should be correct. In the above expressions, the conventional definition of the hydraulic diameter $D_H = 4\,A/P = 2\,\text{Hw}/(H+w)$ is used.

Fig. 7 illustrates the variation of the predicted heat transfer coefficient within an individual channel with increasing volumetric flow rate and different channel heights for a fixed number of channels, $N = 100$ (and thus a fixed channel width of $w = 150\ \mu$m). For a given volumetric flow rate the heat transfer coefficient decreases with increasing channel height/hydraulic diameter. This is due to the reduced velocities associated with the larger channel cross-sectional areas. The figure also illustrates the expected trend that, for a given channel height, the heat transfer coefficient increases with increasing volumetric flow rate. However, it is also evident that the rate of increase of h with $\dot{V}$ increases with decreasing channel height/hydraulic diameter.

Fig. 8 shows the variation of the heat transfer coefficient within a single channel with the total volumetric flow rate

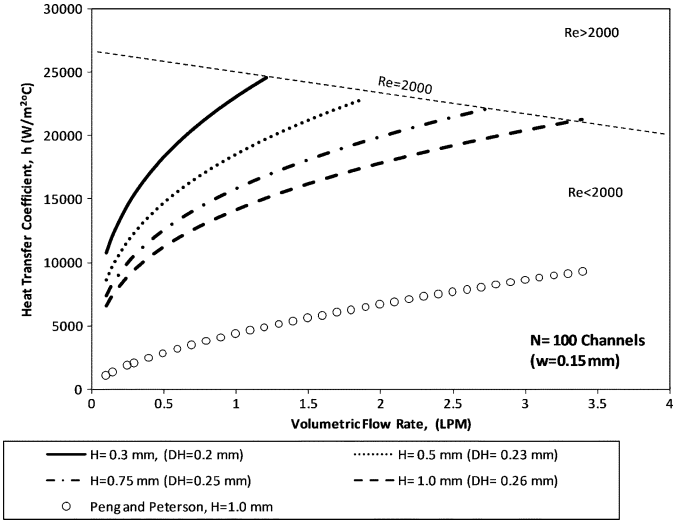

Fig. 7. Variation of the heat transfer coefficient with the total volumetric flow rate and microchannel height for $N = 100$ microchannels.

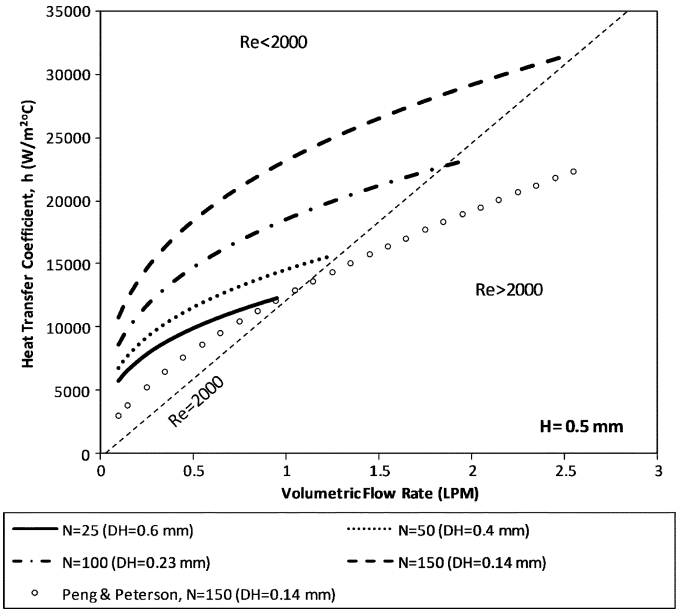

Fig. 8. Variation of the heat transfer coefficient with the total volumetric flow rate and microchannel populations for a fixed channel height of $H = 0.5$ mm.

and microchannel populations for a fixed channel height of $H = 0.5$ mm. The figure highlights that the heat transfer coefficient decreases when the number of channels populating the surface is decreased. Again, widening the channels incurs an increase in the cross-sectional area of the channel with a corresponding reduction in the flow velocity and heat transfer. It is also evident that the sensitivity to changes in N become much more pronounced for smaller hydraulic diameters, i.e., for thin channels.

For comparison purposes, the microchannel heat transfer correlation developed by Peng and Peterson [28] is also plotted in Figs. 7 and 8 for a channel height of $H = 1.0$ mm and a microchannel population of $N = 150$, respectively. Clearly, there is a large discrepancy between the predictions of the macrochannel and the microchannel correlations with the Peng

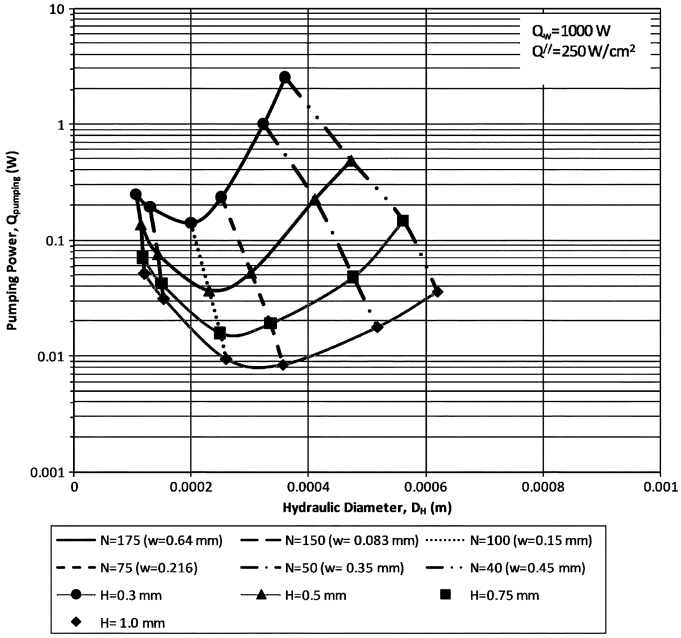

Fig. 9. Variation of the pumping power with hydraulic diameter for a heat flux of 250 W/cm^2.

and Peterson correlation predicting values significantly lower than the Sieder and Tate correlation. Very similar results are obtained using the Wang and Peng [29] correlation.

The pumping power requirement for varying microchannel hydraulic diameter and population is illustrated in Fig. 9 for a heat flux of $q''_w = 250$ W/cm^2. First, it is apparent that for a fixed channel height, a local minimum is observed for increasing hydraulic diameter. For the parameter range tested, this local minimum is not particularly sensitive to the channel height and exists in the area of $D_H \sim 300\ \mu$m. However, the local minimum decreases by an order of magnitude from $Q_{\text{pumping}} \sim 0.15$ W to $Q_{\text{pumping}} \sim 0.008$ W within the range $300\ \mu\text{m} \leq H \leq 1000\ \mu$m, which is significant. Even still, compared with the 1000 W of heat dissipation from the electronic component this power draw is not significant. On either side of the local minimum, Q_{pumping} increases very steeply. However, as D_H increases the flow will eventually become turbulent and tend to offset the rate at which Q_{pumping} escalates. In general, it is evident that to achieve the target heat transfer of $q''_w = 250$ W/cm^2 with a wall temperature of $T_w = 85\ ^\circ$C, taller channels with a hydraulic diameter in the range of $200\ \mu\text{m} \leq D_H \leq 300\ \mu$m are ideal if the aim is to minimize the pumping power consumption.

III. Comparison Between Microchannel and Impinging Jet Heat Sinks

This section will outline a general comparison between the thermal–hydraulic performance characteristics of impinging liquid jet arrays and liquid microchannels. In particular, the general response of the systems to changes in geometric design parameters will be detailed since reducing the physical scale of the device can greatly increase the complexity of manufacture and thus the cost of the overall thermal management solution. Furthermore, the perpetual operating cost of the heat sink will be characterized by considering the pumping power

requirement to achieve a given heat transfer target. Finally, some general comments regarding the practicalities of the two technologies will be made.

A comparison of Figs. 3 and 7 shows that, for the range of parameters considered in this investigation, the impinging jets are generally capable of producing considerably higher heat transfer coefficients compared with the microchannels. For example, for a $D_H = d = 0.3$ mm and a volumetric flow rate of $\dot{V} = 4$ LPM, the 100 microjets are capable of achieving a surface average heat transfer coefficient of $h{\sim}115\,000$ W/m$^{2\circ}$C, whereas 100 microchannels with a comparable $D_H = 0.26$ mm will achieve approximately $h{\sim}20\,000$ W/m $^{2\circ}$C. It is also evident that the heat transfer to the impinging jets is far less sensitive to changes the hydraulic diameter compared to the microchannels.

As illustrated in Fig. 5, increasing the population of impinging jets decreases the heat transfer coefficient due to an overall decrease in the jet velocity. Furthermore, for a fixed $\dot{V}$ the rate at which h escalates decreases with increasing N. For the microchannel heat sinks the opposite trend is observed. Fig. 8 shows that increasing the number of channels tends to increase the heat transfer coefficient since, for a fixed channel height, the decrease in the cross-sectional area causes an increase in the liquid velocity within the channel. In contrast with the impinging jet arrays, for a fixed $\dot{V}$ the rate at which h escalates increases with increasing N.

Although the microchannels cannot achieve as high heat transfer coefficients, the effective heat transfer area can be considerably larger due to the extended surface area of the walls of the channels. It is thus better to compare the thermal resistances of the two systems instead of the heat transfer coefficients. For the impinging jet (IJ) system the thermal resistance is characterized as

$$R_{\mathrm{IJ}} = \frac{1}{hA_w}. \tag{18}$$

Here, $A_w = 0.0004$ m^2 is the surface area of the test surface. The thermal resistance of the microchannel (MC) heat sink is given by

$$R_{\mathrm{MC}} = \frac{w+t}{h(w+2H)A_w}. \tag{19}$$

Equation (19) is obtained by assuming that the resistances resulting from heat flow from the base of the channel and through the fins, with 100% fin efficiency, act thermally in parallel. Equations (18) and (19) are plotted in Fig. 10 for a representative range of parameters for both impinging jets and microchannels. The figure shows that although the microchannels have lower heat transfer coefficients they can achieve thermal resistance values that are as good if not better than the impinging jet counterpart, although it must be noted that the R_{MC} prediction will be considerably higher if the Peng and Peterson [28] or Wang and Peng [29] correlations were used. Even still, regarding the overall thermal resistance, both liquid cooling strategies are comparable with thermal resistance values typically below 0.1°C/W. In particular, for the test case under study here, the thermal resistance required to achieve the given thermal constraints is $R_{\mathrm{TH}} = 0.055$ °C/W. This being the case, both heat sink technologies can easily achieve this target.

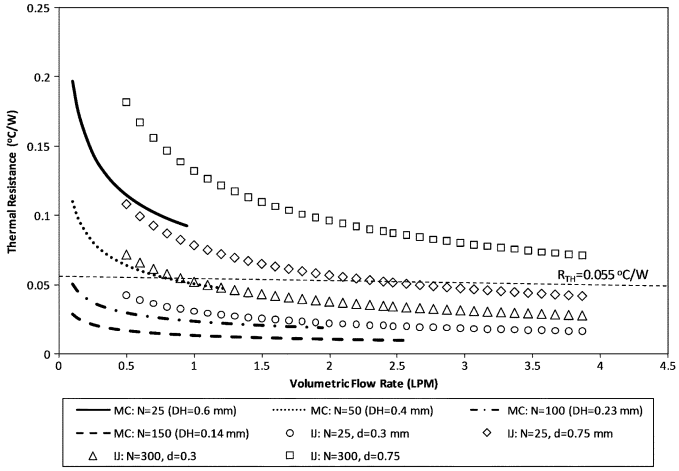

Fig. 10. Thermal resistance versus volumetric flow rate for both the microchannel (MC) and impinging jet (IJ) heat sinks.

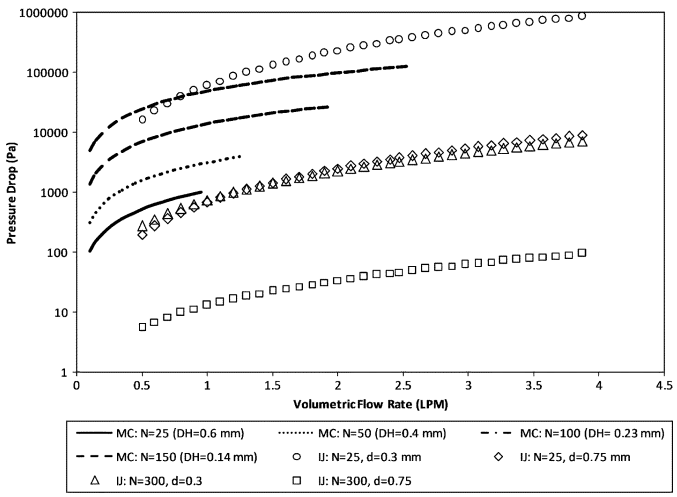

Fig. 11. Pressure drop versus volumetric flow rate for both the microchannel (MC) and impinging jet (IJ) heat sinks.

The pressure drop requirements for the identical conditions of the data in Fig. 10 are plotted in Fig. 11. In general, it can be said that the pressure drop of the impinging jets vary more drastically over the range of parameters tested. For the lowest population of $d = 0.3$-mm jets the very high velocities require an extreme pressure drop, being of the order of $\Delta P{\sim}8$ atm. However, increasing the number of jets can reduce the pressure drop by two orders of magnitude without a severe increase in the thermal resistance, as is evident in Fig. 10. Fig. 11 also shows that the microchannels in Fig. 10 that achieve the $R_{\mathrm{TH}} = 0.055\,^{\circ}$C/W threshold have associated with them a considerable pressure drop whereas, apart from the case discussed above, the impinging jets do not

The long-term power cost of electronic thermal management hardware is becoming an ever greater concern as the energy consumption and electricity costs escalate. An optimized thermal management solution should achieve the required

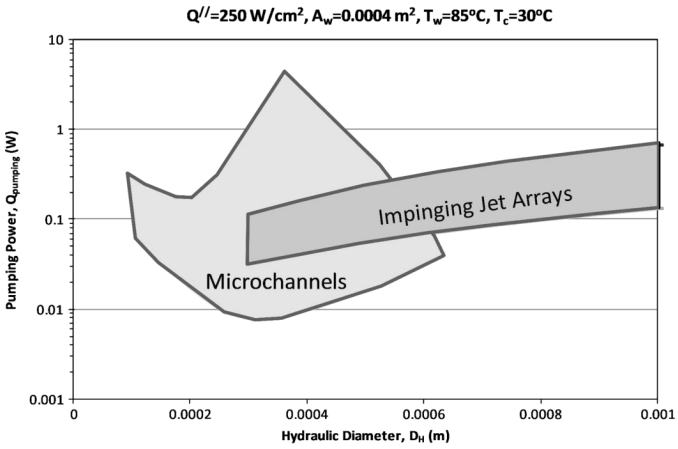

Fig. 12. Pumping power–hydraulic diameter map for the microchannel and impinging jet heat sinks.

thermal goals with the minimum pumping power. As an illustrative example, the thermal constraints for this investigation are $Q'' = 250$ W/cm^2, $A_w = 0.0004\text{m}^2, T_w = 85$ °C, and $T_c = 30$ °C. Fig. 12 is a map of the test conditions applied to the microchannel and jet arrays in this study. It is essentially a combination of the information detailed in Figs. 5 and 9. For the range of parameters studied, it is evident that jet impingement and microchannel cooling both offer adequate performance with regard to pumping power. Although the microchannels generally require a higher pressure drop, this is offset by the fact that the microchannels can achieve the target thermal resistance with a much lower volumetric flow rate compared with the impinging jets. However, the higher volumetric flow rate associated with the impinging jet arrays for the same or comparable pumping power may in fact be desirable since the liquid temperature rise along the heat sink will not be as severe thus offering improved temperature uniformity. Furthermore, a lower operating pressure is desirable from a cost and reliability point of view.

For both heat sinks, power consumptions less than 0.1 W are achievable. This results in coefficients of performance in excess of 10 000 which, from a power management standpoint, is exceptional. Although microchannels are predicted to have pumping powers of the order of $Q_{\text{pumping}} \sim 0.01$ W, it must again be reiterated that this is the nonconservative estimate and the power consumption will likely be higher once more accurate and universal heat transfer and friction factor correlations are developed.

Another interesting detail of Fig. 12 is that for a comparable range of characteristic length and flow scales, the impinging jets encompass a significantly smaller area on the map, especially considering the logarithmic vertical scale. It can thus be concluded that impinging jet heat sinks are far less sensitive to changes in the system environment. This may be a very important design consideration if factors such as manufacturing tolerances and fouling are taken into consideration. For the microchannels, small changes in the channel dimension can result in a disproportionate increase in the pumping power, whereas this is not as severe for the impinging jet solution.

From the discussion above, it is somewhat difficult to distinguish between the two liquid cooling strategies since they both achieve the required thermal performance with very small energy requirements. Thus, the choice of the appropriate cooling strategy will likely be decided by other more practical considerations. First off, single-phase microchannel heat sinks offer the potential of extremely high heat removal rates with very low pumping power and are extremely compact and low-profile. As a result, they are ideal for electronics thermal management and have thus received considerable attention in the last 15 years. However, considering the disagreement with regard to predictions of the friction factor and heat transfer in the open literature, the thermal–hydraulic performance is difficult to accurately predict which leads to uncertainty in modelling and design. Another drawback of microchannel heat sinks is the large axial temperature gradients that develop in the device, due to the singular direction of the flow. Although impinging jet heat transfer has not received near as much attention by the research community, the measurements that are available show good consistency for both heat transfer and pressure drop for a broad range of experimental conditions [11]. Also, from a practical thermal management standpoint, the fact that impinging jets tend to operate at lower pressures and higher flow rates, i.e., better temperature uniformity, and are far less sensitive to changes in the system environment, would indicate that until two-phase microchannel technology is mature enough, this may be the desired solution for single-phase liquid cooling of high-power electronics. Furthermore, as discussed previously, the pressure drop across the jet orifice plates are largely due to the entrance and exit conditions, whereas microchannel pressure drop is dictated primarily by frictional losses within the channels. As a result, significant reductions in the required pressure drop and pumping power $(\sim 20\%)$ can be achieved with simple modifications to the jet orifice entrance and exit conditions [12]–[16]. For microchannels, techniques for skin friction reduction such as ensuring extremely smooth surfaces or applying special coatings must be employed for pressure drop reduction [30]. Another beneficial aspect of impinging jets is that the orifices can be arranged strategically to concentrate jets in areas of high local heat flux which makes them ideal for hot-spot targeting, whereas microchannels are a more global cooling strategy.

From a practical engineering and electronics packaging standpoint, the thermal hardware solution should not incur a significant cost compared with the cost of the overall electronic device. This is likely one of the main drivers towards the massive effort being put forth to extend the useful life of the simple fan-fin air cooling technologies such as reducing fan noise, improving TIMs and heat spreading, as well as improving the air flow within fin banks. However, there is a limit beyond which liquid cooling strategies will be necessary. As a water-block type of solution, microchannel heat sinks can be manufactured using conventional micromanufacturing techniques such as micromilling or microforming which makes them a potentially affordable option. However, for direct liquid contact cooling, where the microchannel is integrated onto the silicon chip, a much more complex manufacturing technique is required which will adversely affect the cost impact of the thermal management hardware on the electronic device. Furthermore, integrating the

thermal management solution and the electronics eliminates the possibility of replacing faulty or deteriorating thermal management hardware. Considering the level of integration of electronic packages that are currently being developed, this can adversely affect long term maintenance costs as well as device reliability.

On the other hand, impinging liquid jet array heat sinks will likely be much cheaper since the nozzle plates can be manufactured at a much reduced cost since the simple array of holes can be formed in the nozzle plate using well established and highly automated manufacturing techniques such as drilling, punching, or possibly even injection moulding. Furthermore, since the nozzle plate is an external piece of hardware, i.e., not integrated on the chip, the quality control of the electronics and the heat sink are separate which should decrease cost and increase reliability. The externally fixed impinging jet nozzle also offers the possibility of future replacement and/or refurbishment.

IV. Conclusion

Single-phase liquid microchannel and confined-submerged impinging jet heat sinks have been compared for a similar range of geometric and flow parameters. With regard to heat transfer, liquid impinging jets perform better with decreasing jet diameter and jet population as a result of the increased jet velocity. However, decreasing the jet diameter and increasing the jet population reduces the pumping power required to achieve a given thermal constraint.

The performance of microchannel heat sinks have been considered for the case which tends to over-predict the heat transfer performance. The calculations indicate that the heat transfer coefficient is very sensitive to changes in the characteristic hydraulic diameter of the channel with the heat transfer coefficient decreasing with the hydraulic diameter of the rectangular channels.

In general, the heat transfer coefficient that is realizable for microchannels is considerably less than for impinging jet arrays. However, the larger surface area that is available with the microchannels tends to provide comparable if not lower thermal resistance values. Also, the pressure drop across the channels is typically higher than the impinging jets though at lower volumetric flow rates which results in exceptionally low pumping power for a target thermal performance. Even still, impinging jet arrays can also achieve the target thermal performance with very low pumping power albeit at higher volumetric flow rates which will provide a more uniform surface cooling.

With regard to the overall thermal performance of the two single-phase cooling techniques, it is difficult to differentiate between the two since they can both achieve very high heat removal rates with minimal energy cost. However, practical considerations such as pressure drop reduction, temperature uniformity, hot-spot targeting, and ease of manufacture tend to indicate that impinging liquid jet array heat sinks may be the method of choice for affordable, energy efficient, and reliable liquid-cooled thermal hardware for the next generation of high-powered electronic devices and packages.

References

[1] V. Natarajan, "Thermal challenges in 3-D stacked packaging," in *Proc. 13th THERMINIC Workshop*, Budapest, Hungary, Sep. 17–19, 2007.

[2] M. Fabbri, S. Jiang, and V. K. Dhir, "A comparative study of cooling of high power density electronics using sprays and microjets," *J. Heat Transfer*, vol. 127, pp. 38–48, 2005.

[3] R. Schmidt, "Liquid cooling is back," *Electron. Cooling*, vol. 11, no. 3, pp. 34–38, Aug. 2005.

[4] B. Smith, T. Brunschwiler, and B. Michel, "Utility of transient testing to characterize thermal interface materials," in *Proc. 13th THERMINIC Workshop*, Budapest, Hungary, Sep. 17–19, 2007, pp. 6–11.

[5] R. Linderman, T. Brunschwiler, B. Smith, and B. Michel, "High-performance thermal interface technology overview," in *Proc. 13th THERMINIC Workshop*, Budapest, Hungary, Sep. 17–19, 2007, pp. 129–134.

[6] F. P. Incropera and D. P. DeWitt, *Liquid Cooling of Electronic Devices by Single-Phase Convection*. New York: Wiley, 1999.

[7] L. M. Jiji and Z. Dagan, , W. Aung, Ed., "Experimental investigation of single-phase multijet impingement cooling of an array of microelectronic heat sources," in *Cooling Technology for Electronic Equipment*. Washington, DC: Hemisphere, 1988, pp. 333–351.

[8] Y. Pan and B. W. Webb, "Heat transfer characteristics of arrays of free-surface liquid jets," *J. Heat Transfer*, vol. 117, pp. 878–883, 1995.

[9] D. J. Womac, F. P. Incropera, and S. Ramadhyani, "Correlating equations for impingement cooling of small heat sources with multiple circular liquid jets," *J. Heat Transfer*, vol. 116, pp. 482–486, 1994.

[10] M. Fabbri and V. K. Dhir, "Optimized heat transfer for high power electronics cooling using arrays of microjets," *J. Heat Transfer*, vol. 127, pp. 760–769, 2005.

[11] A. J. Robinson and E. Schnitzler, "An experimental investigation of free and submerged miniature liquid jet array impingement heat transfer," *Exp. Thermal Fluid Sci.*, vol. 32, pp. 1–13, 2007.

[12] L. A. Brignoni and S. V. Garimella, "Effects of nozzle-inlet chamfering on pressure drop and heat transfer in confined air jet impingement," *Int. J. Heat Mass Transfer*, vol. 43, pp. 1133–1139, 2000.

[13] B. Whelan and A. J. Robinson, "The effect of nozzle geometry on pressure drop and heat transfer to free surface liquid jet arrays," in *ASME-JSME Thermal Eng. Summer Heat Transfer Conf.*, Vancouver, DC, Canada, 2007, Paper no. HT2007-32384.

[14] B. Whelan and A. J. Robinson, "Nozzle geometry effects in liquid jet array impingement," *Appl. Thermal Eng.*, 2009, doi:10.1016/j.applthermaleng.2008.11.003, to be published.

[15] B. Whelan and A. J. Robinson, "Effect of nozzle geometry on pressure drop and heat transfer to both free-surface and submerged liquid jet arrays," in *Proc. Eurotherm*, Eindhoven, The Netherlands, May 18–22, 2008, Paper FCV3.

[16] A. Royne and C. J. Dey, "Effect of nozzle geometry on pressure drop and heat transfer in submerged jet arrays," *Int. J. Heat Mass Transfer*, vol. 49, pp. 800–804, 2006.

[17] G. L. Morini, "Single-phase convective heat transfer in microchannels: A review of experimental results," *Int. J. Thermal Sci.*, vol. 43, pp. 631–651, 2004.

[18] I. Hassan, P. Phutthavong, and M. Abdelgawad, "Microchannel heat sinks: An overview of the state-of-the-art," *Microscale Thermophys. Eng.*, vol. 8, pp. 183–205, 2004.

[19] H. Herwig and O. Hausner, "Critical view on 'new results in microfluid mechanics': An example," *Int. J. Heat Mass Transfer*, vol. 46, pp. 935–937, 2003.

[20] J. Li, G. P. Peterson, and P. Cheng, "Three-dimensional analysis of heat transfer in a micro-heat sink with single phase flow," *Int. J. Heat Mass Transfer*, vol. 47, no. 19–20, pp. 4215–4231, 2004.

[21] X. Li, X. Huai, Y. Tao, and H. Chen, "Effects of thermal property variation on the liquid flow and heat transfer in microchannel heat sinks," *Appl. Thermal Eng.*, vol. 25, pp. 2803–2814, 2007.

[22] C. P. Tso and S. P. Mahulikar, "Experimental verification of the role of Brinkman number in microchannels using local parameters," *Int. J. Heat Mass Transfer*, vol. 43, pp. 1837–1849, 2000.

[23] E. N. Seider and C. E. Tate, "Heat transfer and pressure drop of liquids in tubes," *Ind. Eng. Chem.*, vol. 28, pp. 1429–1435, 1936.

[24] H. Hausen, *Heat Transfer in Counter Flow, Parallel Flow and Cross Flow*. New York: McGraw-Hill, 1983.

[25] F. P. Incropera and D. P. DeWitt, *Fundamentals of Heat and Mass Transfer*, 4th ed. New York: Wiley, 1996.

[26] F. Kreith and M. S. Bohn, *Principles of Heat Transfer*, 5th ed. St. Paul, MN: West, 1993.

[27] J. S. Bintoro, A. Akbarzadeh, and M. Mochizuki, "A closed-loop electronics cooling by implementing single phase impinging jet and mini channels heat exchanger," *Appl. Thermal Eng.*, vol. 25, pp. 2740–2753, 2005.

[28] C. Harris, M. Despa, and K. Kelly, "Design and fabrication of a cross flow micro heat exchanger," *J. Microelecromech. Syst.*, vol. 9, no. 4, pp. 502–508, 2000.

[29] X. F. Peng and G. P. Peterson, "Convective heat transfer and flow friction for water flow in microchannel structures," *Int. J. Heat Mass Transfer*, vol. 39, pp. 2599–2608, 1996.

[30] B. X. Wang and X. F. Peng, "Experimental investigation of liquid forced-convection heat transfer through microchannels," *Int. J. Heat Mass Transfer*, vol. 37, no. 1, pp. 73–82, 1994.

[31] R. Enright, C. Eason, C. T. Dalton, M. Hodes, T. Salamon, P. Kolodner, and T. Krupenkin, "Friction factors and Nusselt numbers in microchannels with superhydrophobic walls," in *Proc. 4th ICNMM2006*, Limerick, Ireland, 2006, pp. 599–609.

Anthony J. Robinson received the Ph.D. degree from McMaster University, Hamilton, ON, Canada, in 2002.

He is a Lecturer in fluid mechanics and heat transfer at Trinity College Dublin, Dublin, Ireland. His research interests are in the field of nucleate pool boiling, two-phase flow and heat transfer, thermal interface materials, and liquid cooling of electronics.